N94-31034

THE IMPACT OF LDEF RESULTS ON THE SPACE APPLICATION OF METAL MATRIX COMPOSITES*

Gary L. Steckel
The Aerospace Corporation
El Segundo, CA 90245
Phone: 310/336-7116, Fax: 310/336-7055

Tuyen D. Le
The Aerospace Corporation
Phone: 310/336-7864, Fax: 310/336-7055

SUMMARY

Over 200 graphite/aluminum and graphite/magnesium composites were flown on the leading and trailing edges of LDEF on the Advanced Composites Experiment. The performance of these composites was evaluated by performing scanning electron microscopy and x-ray photoelectron spectroscopy of exposed surfaces, optical microscopy of cross sections, and on-orbit and postflight thermal expansion measurements. Graphite/aluminum and graphite/magnesium were found to be superior to graphite/polymer matrix composites in that they are inherently resistant to atomic oxygen and are less susceptible to thermal cycling induced microcracking. The surface foils on graphite/aluminum and graphite/magnesium protect the graphite fibers from atomic oxygen and from impact damage from small micrometeoroid or space debris particles. However, the surface foils were found to be susceptible to thermal fatigue cracking arising from contamination embrittlement, surface oxidation, or stress risers. Thus, the experiment reinforced requirements for carefully protecting these composites from prelaunch oxidation or corrosion, avoiding spacecraft contamination, and designing composite structures to minimize stress concentrations. On-orbit strain measurements demonstrated the importance of through-thickness thermal conductivity in composites to minimize thermal distortions arising from thermal gradients. Because of the high thermal conductivity of aluminum, thermal distortions were greatly reduced in the LDEF thermal environment for graphite/aluminum as compared to graphite/magnesium and graphite/polymer composites. The thermal expansion behavior of graphite/aluminum and graphite/magnesium was stabilized by on-orbit thermal cycling in the same manner as observed in laboratory tests.

EXPERIMENT DESCRIPTION

Nearly 500 samples of metal matrix, glass matrix, and polymer matrix composites were flown on LDEF Experiment M0003-10, "The Advanced Composites Experiment," a subexperiment of LDEF Experiment M0003, "Space Environmental Effects on Spacecraft Materials." The subexperiment is a joint effort between government and industry with Air Force Wright Laboratory, Flight

*Funding for this effort was processed through Air Force Space Systems Division Contract F04701-88-C-0089 under an interagency agreement with Air Force Wright Laboratory.

Dynamics Laboratory, and The Aerospace Corporation, Mechanics and Materials Technology Center, serving as experimenters. Each organization that participated in the experiment supplied a set of samples which were integrated into the overall experiment by The Aerospace Corporation. Following postflight deintegration, the samples were returned to the suppliers for analysis. In this paper, the most significant results for the metal matrix composites will be summarized. The metal matrix composites included primarily graphite fiber-reinforced aluminum and magnesium and were supplied and evaluated by The Aerospace Corporation.

The polymer matrix composites in the experiment included graphite/epoxy, graphite/polysulfone, and graphite/polyimide composites with and/or without various thermal control or protective coatings. These composites were supplied by General Dynamics Space Systems Division, Lockheed Missiles and Space Company, Boeing Aerospace & Electronics, and McDonnell Douglas Space Systems Company. The results for the polymer matrix composites in the experiment were presented at the 1991 LDEF Materials Workshop (ref. 1). The results were consistent with the findings of other experiments for polymer matrix composites that are included in this publication (refs. 2,3). The glass matrix composites were also reinforced with graphite fibers and were provided by United Technologies Research Center. They were uncoated and had either GY70 or Celion 6000 graphite fibers in a borosilicate glass matrix. Tredway and Prewo (ref. 4) evaluated the effects of the space exposure on graphite/glass composites from visual observations, optical microscopy, scanning and transmission electron microscopy, and diffuse reflectance, thermal expansion, and mechanical property measurements. They found that graphite/glass composites were essentially unaffected by the extended space exposure on LDEF. Since the impact of the LDEF results on the space application of the polymer and glass matrix composites was discussed in references 2 to 4, the results for these composites were omitted from this paper.

The experiment occupied approximately one-sixth of a 6-in deep peripheral tray on both the leading and trailing edges of LDEF. The trays were located on LDEF Bay D, Row 4 on the trailing edge and Bay D, Row 8 on the leading edge. The samples were mounted on both sides of cassettes with one side (Deck A) exposed to the space environment and the other side (Deck B) facing inward. The environments for the samples mounted on the leading and trailing A decks were similar except those on the leading edge were also exposed to relatively high fluxes of atmospheric constituents, primarily atomic oxygen. Although the samples on the B decks were not exposed to the radiation environment, the experiment design was such that they experienced thermal excursions similar to those of the exposure samples. The sample cassettes were decoupled from LDEF in order to maximize the thermal excursions. For most materials, at least one sample was located on each deck and additional samples were maintained in a laboratory environment. Although this was essentially a passive experiment, one or more samples of most classes of metal and polymer matrix composites were instrumented with thermistors and strain gauges to monitor the thermal excursions on the leading and trailing edges and the resulting dimensional changes.

COMPOSITE MATERIALS

Most of the composite samples were 3.5 by 0.5 in (8.9 by 1.3 cm) strips. There were also a limited number of 1-in (2.5-cm) diameter mirror samples, a few 2.4- by 0.5-in (6.1- by 1.3-cm) strips and several continuous fiber-reinforced wires. Most of the wires were approximately 0.025 in (0.064 cm) in diameter. The metal matrix composites are listed in Table 1. The graphite/aluminum (Gr/Al) strip and mirror samples included three different graphite fibers and two different alloy

matrices. These composites also had four different lay-ups. The graphite/magnesium (Gr/Mg) strips and mirrors included P100/EZ33A/AZ31B and P100/AZ91C/AZ61A composites. The samples for LDEF were prepared during the early stages of the development of graphite/magnesium. At that time, P100/EZ33A/AZ31B was considered a leading candidate system for space applications. However, it was subsequently discovered that poor strength properties were inherent in this system and it was replaced by the P100/AZ91C/AZ61A system. Therefore, several P100/AZ91C/AZ61A samples were added to the test matrix shortly before the experiment trays were delivered to NASA. These samples are of great interest as they are representative of the current state-of-the-art for graphite/magnesium. The silicon carbide/aluminum composites included both discontinuous whisker-reinforced and continuous fiber-reinforced strips. The metal matrix wires included five fiber-matrix combinations for graphite/aluminum, three fiber-matrix combinations for graphite/magnesium, and Nicalon SiC fiber-reinforced 6061 aluminum. Most of the wires were prepared by infiltrating a single row of fibers with the molten matrix alloy, but in some cases, several rows were infiltrated to form a larger diameter wire.

The detailed results for the Gr/Al and Gr/Mg composites were presented in earlier papers (refs. 5–7). Therefore only the most significant results relative to the space application of these composites will be reviewed. The results of surface observations, microscopy of cross sections, the on-orbit temperature and strain measurements, and postflight thermal expansion measurements on Gr/Al and Gr/Mg are included. Evaluation of the silicon carbide/aluminum samples is still in progress and no results will be presented for these composites.

VISUAL AND MICROSCOPIC OBSERVATIONS FOR GR/AL AND GR/MG

A postflight photograph of the exposed side of the leading edge cassette is shown in Figure 1. The mirror samples were mounted in the upper right corner of the cassette with the metal matrix wires located immediately to the left of the mirrors and the 3.5-in by 0.5-in strips filling the remainder of the cassette. It was noted that all of the composites survived in excellent physical condition. Surface roughening due to atomic oxygen erosion for uncoated organic matrix composites mounted on the exposed leading edge was the only significant visible damage. However, the erosion depth appeared to be shallow relative to the overall thickness of the affected composites. Contamination was evident on both the leading and trailing edges. For example, a large contaminated area is apparent on seven samples in the upper left corner of the photograph in Figure 1. It will be shown below that contaminants may have induced surface cracks in some of the Gr/Al composites.

A micrometeoroid/debris crater on a Gr/Al composite is shown in Figure 2. This crater is typical of those observed on both Gr/Al and Gr/Mg. Since Gr/Al has an aluminum alloy surface foil, the crater has the same appearance as for monolithic aluminum. A cross section of this crater shows that it extended completely through the 0.004 in (0.010 cm) 2024 aluminum surface foil, but did not extend into the underlying graphite fiber-reinforced interior. This may imply that penetration through the foil is much easier than through the fiber-reinforced region of the composite, but may also be the characteristic depth of penetration into aluminum for this particular size of impact particle. Most of the craters observed on Gr/Al and Gr/Mg composites were approximately the same size. Thus, the effects of particle size on the penetration depth could not be determined. Perhaps the most significant observation in Figure 2 is the presence of a delamination of the surface foil over an area approximately three times the crater diameter. It is not known whether the delamination occurred due to the impact energy or formed later due to thermal fatigue. Surface foil delaminations affect important

through-thickness properties, such as the thermal conductivity. In addition, most of the transverse strength of Gr/Al and Gr/Mg is provided by the surface foil. Large foil delaminations could therefore have serious consequences on the performance of these composites. Thus, if the delaminations propagate due to thermal fatigue, they could reach much larger sizes during extended missions and have adverse effects. Additional studies are needed to determine whether the delaminations form due to the impact or if they develop and/or propagate during subsequent thermal cycling.

Etching of cross sections of Gr/Al and Gr/Mg flight samples produced matrix darkening in the fiber-reinforced regions as shown in Figure 2. The dark etching is an indication of plastic deformation of the matrix. This is not surprising since the coefficient of thermal expansion mismatch between the graphite fibers and matrix induces high stresses in the matrix during thermal cycling. Nevertheless, there was no evidence of matrix microcracking in any Gr/Al or Gr/Mg composites. Since the samples were subjected to over 33,000 thermal cycles, this indicates that these composites have excellent resistance to thermal fatigue for the LDEF thermal environment. Extensive thermal fatigue cracking was observed, however, on the surface foils of selected GY70/201/2024 Gr/Al samples (Fig. 3). This was surprising since the thermal stresses should be lower within the surface foils than within the fiber-reinforced regions of the composites. However, further inspection revealed that the cracks were always associated with a surface contaminant that was clearly visible on several trailing edge samples that had been mounted adjacent to one another. X-ray Photoelectron Spectroscopy (XPS)† showed the presence of silicon and oxygen, probably from on-orbit silicone contamination. The cracks probably initiated in a brittle oxide or aluminum silicate layer on the sample surface. Once the cracks were initiated, they propagated into the bulk of the foil. In some cases (Fig. 3), the cracks propagated completely through the surface foil. However, there was no evidence of the cracks extending into the underlying Gr/Al region or along the interface between this region and the foil.

Less severe, isolated fatigue cracks were also observed on a few GY70/201/2024 Gr/Al composites. These cracks were always associated with surface defects such as surface foil blemishes, micrometeoroid craters or engraved sample identification numbers (Fig. 4). Apparently, these defects acted as stress concentrators and initiated thermal fatigue cracks. All of the Gr/Al composites that had surface foil cracks, due to either contamination or stress risers, had 2024 surface foils. No composites having 6061 surface foils showed any evidence of foil cracking. The composites having 6061 surface foils were heat treated to a T6 condition, whereas those having 2024 foils were in the as-fabricated condition. Thus, the 6061 foils probably had a higher yield strength, which would also tend to increase the fatigue life of the 6061 foils relative to the 2024 foils (ref. 8). These observations are consistent with postflight microhardness measurements, which verified that the 6061 foils were significantly harder than the 2024 foils.

Surface foil cracks were also observed on several Gr/Mg composites. In this case, all of the cracked samples had a very rough, mottled surface appearance (Fig. 5), which XPS indicated was due to extensive surface oxidation. Several observations concerning the oxidation and foil cracking were made from an evaluation of all of the P100/AZ91C/AZ61A Gr/Mg composites. These included samples from two panels, one having a single-ply, unidirectional lay-up and a second panel having four plies in a $(\pm 10°)_S$ lay-up. The unidirectional panel had been stored in a laboratory for 2 years before we decided to use it for LDEF. The surface of the panel was heavily oxidized and required abrading to prepare samples having clean surfaces. The resulting rough surface was, however, susceptible to additional oxidation, which was observed for all samples from this panel that were

†C.S. Hemminger was responsible for the x-ray photoelectron spectroscopy and its interpretation.

mounted on the A decks for both the leading and trailing edges. All of these samples also had extensive surface foil cracking. Samples mounted on the interior B decks showed much less oxidation and no foil cracking. Since the degree of oxidation was the same on the leading and trailing edges, we believe that these observations are indicative of prelaunch oxidation. The four-ply panel was prepared for LDEF shortly before the experiment trays were delivered to NASA. This panel had very smooth surfaces that were not as prone to oxidation. As a result, the flight samples showed only light oxidation and no surface foil cracking. Thus, it was concluded that the surface foil cracking on Gr/Mg was due to the formation of a brittle oxide layer that formed prior to launch, but can be eliminated by the application of suitable prelaunch handling and surface preparation procedures.

THERMAL EXPANSION BEHAVIOR OF GR/AL AND GR/MG

The effects of the long-term space exposure on the thermal expansion behavior of Gr/Al and Gr/Mg were evaluated by: (1) analyzing the flight data that was recorded on-orbit to determine the influence of orbital time and orbital heating and cooling conditions, and by (2) postflight laboratory measurements of LDEF samples and laboratory control samples. In this analysis, temperature change versus time, dimensional change versus temperature, coefficient of thermal expansion (CTE), and thermal hysteresis were considered in evaluating the dimensional stability.

Eleven Gr/Al and five Gr/Mg samples were instrumented with thermistors and/or strain gauges to monitor the thermal cycling and associated thermal strains during orbiting. The strain gauges and thermistors were mounted on the back surface of both leading and trailing edge exposure samples. None of the flight control samples were instrumented. The sensors were placed on the back surface to avoid any possible damage caused by atomic oxygen erosion, UV radiation, or micrometeoroid bombardment. The disadvantages of this approach were that any temperature gradients through the thickness of the radiantly heated and cooled samples were undetected, as were any bending deformations associated with temperature gradients. It will be shown that for some materials this had a dominant influence on the data. The strain gauges were mounted to measure the change in dimension along the length of the strips. The data acquisition system was set up to record temperatures and strains during the duration of an orbit once every 107 hours (approximately 78 orbits). Data were collected approximately every three minutes during the selected orbits. The first set of data was collected approximately 44 hours after LDEF was placed into orbit. The data were recorded on magnetic tape until the tape was fully loaded, approximately fourteen months into the flight. No data were recorded during the unplanned final 4.5 years of the flight.

The absolute values of linear thermal expansion in graphite fiber-reinforced composite materials are extremely small, particularly in the direction parallel to the fibers. This requires the use of a high resolution apparatus such as a laser interferometer to make accurate thermal expansion measurements. In this study, a Michelson laser interferometer was utilized for the postflight laboratory measurements. In all cases, thermal cycling was carried out by first heating the sample to the maximum temperature, followed by cooling to the lowest temperature, and then heating back to room temperature. The heating and cooling rates were limited to approximately 1 °C/min (2 °F/min) to ensure thermal equilibrium throughout the sample. For the purpose of comparison with the flight data, the samples were thermal cycled over the same range of temperature that was derived from the flight data analysis.

Plots of the maximum and minimum temperatures for each orbit for which data were taken are shown in Figure 6 for a P100/EZ33A/AZ31B Gr/Mg composite. Large fluctuations in the thermal cycling occurred due to seasonal variations and orbital mechanics. For the flight data analyses, it was desirable to select typical thermal expansion curves for orbits at the beginning, middle, and the end of the recording time. In addition, equivalent temperature ranges for the selected orbits were preferred in order to facilitate comparisons. Therefore, the orbital times indicated by vertical lines on the Figure at approximately 40, 5,000, and 10,000 hours (2, 208, 416 days) after LDEF was placed into orbit were selected for the data analyses. The temperature range for these orbits was approximately –20 to 70 °C (–5 to160 °F), but varied somewhat between the leading and trailing edges and between Gr/Al and Gr/Mg. In general, higher temperatures for these orbits were measured for Gr/Mg versus Gr/Al and for the trailing versus the leading edge.

A listing of all the Gr/Al and Gr/Mg composite systems for which flight data were obtained and analyzed is given in Table 2. The composites for which postflight laboratory measurements were made are also indicated. Note that no flight data were obtained for the P100/201/2024 Gr/Al or P100/AZ91C/AZ61A Gr/Mg composites because of their late addition to the experiment. The results for each of these composites were discussed previously (ref. 7). Only the data for the GY70/201/2024 Gr/Al composites and P100/EZ33A/AZ31B and P100/AZ91C/AZ61A $(\pm 10°)_S$ Gr/Mg composites will be reviewed in this paper.

Figure 7 shows a typical thermal cycle for one orbit and the corresponding dimensional changes plotted as a function of time for a Gr/Al composite on the trailing edge. The temperature plot shows that the initial heating and cooling rates as LDEF came out of or went into the Earth's shadow, respectively, were very rapid, around 7 °F/min. The rates were even higher, around 15 °F/min, on the leading edge. It is reasonable to assume that the heating and cooling rates were even higher on the front surface of the sample, so that a temperature gradient through the sample causing bending deformations would not be surprising. Since Gr/Al has a positive CTE, these bending deformations would tend to reduce the thermal strains measured by a back surface strain gauge. However, the slope changes for the strain in Figure 7 were consistent with those for the temperature. Thus, the through-thickness thermal conductivity of Gr/Al was apparently sufficient to prevent significant thermal distortions for these heating and cooling rates.

In Figure 8, the on-orbit thermal expansion curves are shown for GY70/201/2024 composites mounted on the leading and trailing edges of LDEF. The curves are shown for the three selected orbits (40, 5,000, and 10,000 hours). The thermal expansion behavior was fairly linear with only a small degree of hysteresis. In addition, the thermal expansion was very stable in that it showed no significant change with orbital time. The postflight laboratory data for the same leading and trailing edge GY70/201/2024 samples are shown in Figure 9. The laboratory curves were more linear, suggesting that the flight data may have been somewhat influenced by the rapid on-orbit heating and cooling rates. The trailing edge sample showed a small degree of hysteresis as compared to the leading edge sample in both the flight data and laboratory measurements. This observation is probably due to differences between the two samples, such as slightly different fiber contents, rather than any differences between the leading and trailing edge exposures. Figure 10 compares the thermal expansion curve of a laboratory control sample with the leading edge sample. The thermal expansion behavior of the laboratory control sample was similar to the flight samples except for a small, but readily noticeable, hysteresis loop over the entire temperature range. The reduced hysteresis in the flight samples is probably indicative of strain hardening of the matrix further stabilizing the composites after a few thermal cycles. However, the small degree of hysteresis indicated that even the uncycled, laboratory control samples were quite stable. The P55/6061/6061 composites showed

basically the same behavior, except no hysteresis was observed for the flight or laboratory control samples. The average postflight CTEs measured in the laboratory for the GY70/201/2024, P55/6061/6061, and four-ply P100/201/2024 Gr/Al composite systems are given in Table 3. The CTE was not affected by the extended space exposure for any of the Gr/Al composites. Note that the CTE was much lower for the P100/201/2024 composites because of the more negative CTE of the P100 fiber compared to the P55 and GY70 fibers and the $(\pm 20°)_S$ lay-up. The results indicate that the extended space exposure on LDEF had little effect on the thermal expansion of Gr/Al. Thermal cycling in orbit further stabilized the Gr/Al composites, eliminating thermal hysteresis after less than 40 cycles. Although the rapid temperature changes encountered on LDEF may have had a small effect on the strain measurements, temperature gradients were not sufficient to induce significant bending.

Plots of the temperature and strain gauge response versus time for a Gr/Mg composite are shown in Figure 11. Anomalous behavior was observed for the Gr/Mg composites when the heating or cooling rates were very rapid. This particular Gr/Mg composite had a positive CTE, but when the heating rate became very rapid, the sample appeared to contract instead of expanding. Furthermore, with rapid cooling, the strain increased rather than decreasing. When the heating and cooling rates were relatively slow, the measured strains increased or decreased as anticipated. This behavior is consistent with the development of bending deformations in the strips during the rapid heating and cooling. The thermal conductivity of Gr/Al composites is significantly greater than for Gr/Mg due to the much higher Al matrix conductivity. For example, the conductivities at 70 °F for 6061-T6 Al and AZ91C Mg are 97 and 58 Btu/ft-hr-°F, respectively (ref. 8). The through-thickness conductivities of P100/6061/6061 Gr/Al and P100/AZ91C/AZ61A Gr/Mg composites having fiber contents of approximately 40 vol. percent are around 40 and 20 Btu/ft-h-°F at 70 °F, respectively (ref. 9). In addition, higher heating and cooling rates were measured on the leading and trailing edges for Gr/Mg (20 and 10 °F/min, respectively) than for Gr/Al (15 and 7 °F/min). This would also tend to increase bending deformations in Gr/Mg relative to Gr/Al.

Figure 12 shows the measured strain versus temperature for single-ply P100/EZ33A/AZ31B composites mounted on the leading and trailing edges of LDEF. The postflight thermal expansion curves for these same samples are plotted in Figure 13 along with the curve for a laboratory control sample. Comparing Figures 12 and 13 clearly shows that the flight data were severely altered by the high heating and cooling rates. The interpretation of these data can only be accomplished by performing analyses to calculate the front surface temperatures and bending deformations. Similar problems were encountered for the polymer matrix composites. The thermal conductivity is even lower for these composites. In addition, the polymer matrix composites were thicker and had higher solar absorptance and emittance properties than Gr/Al and Gr/Mg. All of these factors would tend to increase the the through-thickness temperature gradients and the bending deformations in the polymer matrix composites.

The thermal expansion of the laboratory control P100/EZ33A/AZ31B composite in Figure 13 was extremely unstable. The behavior was nonlinear with a large residual thermal strain at room temperature of nearly 300 microstrain. The large residual strain of the material is attributed to yielding of the low-strength matrix alloy. The composite behavior near the cold end of the cycle was dominated by the expansion of the fibers causing yielding in the matrix. This led to an increase in dimension and consequently an open loop with large permanent offset at room temperature. A comparison of the laboratory control sample with the postflight samples showed that the amount of hysteresis decreased remarkably following the on-orbit thermal cycling. The implication is that extensive thermal cycling had a large effect in stabilizing the behavior of the P100/EZ33A/AZ31B

Gr/Mg composites. However, even after over 30,000 thermal cycles on LDEF, the thermal hysteresis could not be cycled out as it was for Gr/Al composites. As discussed above, P100/EZ33A/AZ31B composites have inherently low strength properties due to chemical reactions between the rare Earth elements in the EZ33A matrix alloy and the P100 fibers. These reactions may also affect the matrix and limit its work hardening so that hysteresis in the thermal expansion curves could not be eliminated. It should be noted however that the total dimensional change and average CTE for the Gr/Mg composites were smaller than those for the Gr/Al composites. This is due to the low elastic modulus of the magnesium matrix alloy (6.5 Msi) and the higher modulus and more negative CTE of the P100 fiber as compared to the P55 and GY70 fibers.

Post-flight thermal expansion curves for leading edge and laboratory control samples of the 4-ply, $(\pm 10°)_S$ P100/AZ91C/AZ61A composites are shown in Figure 14. These measurements were made at Composite Optics, Incorporated, over a much broader temperature range than the samples were exposed to on LDEF. The laboratory control and postflight samples had nearly identical curves. Both samples had a hysteresis of around 75 microstrain, but the CTE's were extremely small, around 0.07×10^{-6}/°F. The similarities between the two samples indicated that the thermal expansion was originally quite stable and that extensive thermal cycling over the LDEF temperature range did not have much effect on the thermal expansion over the ±250 °F range. However, making measurements over a broader temperature range than the on-orbit temperatures undoubtedly diminished the stabilizing effects of the thermal cycling. A second set of laboratory control and flight samples need to be evaluated over the LDEF temperature range. This will give a better indication of the stabilizing effect of the LDEF thermal cycling for these low-CTE composites.

CONCLUSIONS

(1) All of the composites flown on LDEF in the Advanced Composites Experiment survived the extended space exposure in excellent physical condition. The only significant visible damage was surface erosion on uncoated polymer matrix composites from atomic oxygen on the leading edge of LDEF. Gr/Al, Gr/Mg, silicon carbide/Al, and graphite/glass composites were not susceptible to atomic oxygen attack.

(2) The largest micrometeoroid or debris craters observed on Gr/Al and Gr/Mg were approximately 0.006 in (150 micrometers) in diameter. Minimal damage was caused to these composites, in part because the aluminum or magnesium surface foils protected the graphite fibers for these small impact particles. However, even small particle impacts can cause localized delamination of the surface foil which may propagate due to subsequent thermal cycling. This could degrade through-thickness properties such as thermal conductivity or transverse properties.

(3) No evidence of any internal microcracking was observed for Gr/Al or Gr/Mg for any of the fiber/matrix combinations or lay-ups flown on LDEF.

(4) Several GY70/201/2024 Gr/Al composites had thermal fatigue cracks within the 2,024 surface foils. These crack appeared to initiate at the outer foil surface. In some instances the cracks extended through the foil, but no cases were observed in which the cracks propagated into the fiber reinforced region of the composite or caused foil delaminations. These cracks were attributed to surface contamination or stress risers such as engraved sample numbers or micrometeoroid craters. No cracks were observed for Gr/Al composites having 6061 Al surface

foils. The presence of these cracks accentuates the need to be very careful in the surface preparation and design of composite structures to minimize stress concentrators and the need to avoid contamination on all spacecraft surfaces.

(5) Fatigue cracking due to prelaunch oxidation was observed on numerous P100/EZ33A/AZ31B and P100/AZ91C/AZ61A Gr/Mg composites. It was shown that this can be prevented by the application of suitable prelaunch handling and surface preparation procedures.

(6) Gr/Al composites showed a stable, linear thermal expansion behavior with near-zero thermal hysteresis over the LDEF temperature range. In contrast, Gr/Mg composites, even after extensive cycling during orbiting, showed nonlinear, unstable behavior with significant hysteresis. However, the hysteresis for Gr/Mg was significantly reduced as compared to the as-fabricated samples. The thermal expansion data for Gr/Mg composites indicated that near-zero CTE over the LDEF temperature range can be obtained and maintained on-orbit. These results are consistent with and validate ground-based thermal cycling test results on Gr/Al and Gr/Mg composites.

(7) The flight data revealed that in the space environment, the temperature distribution in a structure is often time varying or nonuniform due to radiant heating. For a satellite like LDEF in a low Earth orbit with alternating eclipse and sun exposure, the data showed that the materials experienced thermal cycling over varying temperature extremes with different heating and cooling rates depending on the location of samples on the satellite. During a single orbit, the heating and cooling rates could vary from less than 1 °F/min to 20 °F/min when LDEF was going in or out of the Earth's shadow. The maximum heating and cooling rates on the leading edges were nearly twice those on the trailing edge. Bending deformations due to temperature gradients through the thickness of the Gr/Mg and polymer matrix composites were implied from the strain gauge data and attributed to the low thermal conductivity of these composites as compared to Gr/Al. The flight data implies that structures in space are always subjected to nonuniform temperature distributions and thermal conductivity of a material is an important factor in establishing a uniform temperature distribution. Therefore in addition to CTE and thermal hysteresis, thermal conductivity is an important consideration when selecting materials for dimensionally stable space structures.

REFERENCES

1. Steckel, G.L., Cookson, T., and Blair, C.: "Polymer Matrix Composites on LDEF Experiments M0003-9 & 10." *Proceedings of LDEF Materials Workshop '91*, NASA CP-3162, pp. 512–542.

2. Tennyson, R.: "Space Environmental Effects on Composite Structures." *LDEF Materials Results For Spacecraft Applications Conference*, NASA CP- , 1992.

3. George, P.: "Low Earth Orbit Effects on Organic Composite Materials Flown on LDEF." *LDEF Materials Results For Spacecraft Applications Conference*, NASA CP- , 1992.

4. Tredway, W.K. and Prewo, K.M.: "Analysis of the Effect of Space Environmental Exposure on Carbon Fiber Reinforced Glass." United Technologies Research Center Report R91-112542-4, 1991.

5. Steckel, G.L. and Le, T.D.:: "Composites Survive Space Exposure." *Advanced Materials and Processes*, vol. 139, No. 8, 1991, pp. 35–38.

6. Steckel, G.L. and Le, T.D.: "M0003-10: LDEF Advanced Composites Experiment." First LDEF Post-Retrieval Symposium, NASA CP-3134, 1991, pp. 1041–1053.

7. Le, T.D. and Steckel, G.L.: "Thermal Expansion Behavior of LDEF Metal Matrix Composites." Second LDEF Post-Retrieval Symposium, NASA CP-3194, 1992, pp. 67.

8. *Metals Handbook Ninth Edition, Volume 2, Properties and Selection: Nonferrous Alloys and Pure Metals*. American Society For Metals, 1979.

9. Taylor, R.E. and Groot, H.: *Thermophysical Properties of Graphite Aluminum and Graphite Magnesium*, Thermophysical Properties Research Laboratory Report TPRL 330, Purdue University, West Lafayette, IN, 1984.

Table 1. List of metal matrix composites.

MATERIAL DESCRIPTION FIBER/MATRIX/SURFACE FOIL	LAY UP	NUMBER OF SAMPLES LEADING A	LEADING B	TRAILING A	TRAILING B	CONTROL
GRAPHITE/ALUMINUM						
GY70/201/2024 STRIPS	0, 90, OR $(0/\pm60)_S$	15	14	13	18	20
P55/6061/6061 STRIPS	0 OR 90	8	10	8	8	12
P100/201/2024 STRIPS	$(\pm20)_S$	2	2	2	2	2
P100/6061 WIRES	0	4	1	4	1	2
P55/6061 WIRES	0 OR $(0)_5$	8	3	8	3	6
GY70/201 WIRES	$(0)_8$	2	1	2	1	2
T300/6061 WIRES	0	2	1	2	1	2
GRAPHITE/MAGNESIUM						
P100/EZ33A/AZ31B STRIPS	0, 90, OR $(0/\pm60)_S$	9	11	7	8	33
P100/AZ91C/AZ61A STRIPS	0, 90 OR $(\pm10)_S$	6	4	6	6	3
P100/AZ31B WIRES	0	3	1	3	1	2
P100/AZ61A WIRES	0	4	1	4	1	2
P55/AZ91C WIRES	$(0)_5$	3	1	3	1	4
SILICON CARBIDE/ALUMINUM						
SiC_w/2124 STRIPS	DISCONTINUOUS	1	1	1	1	5
SiC_w/6061 STRIPS	DISCONTINUOUS	1	1	1	1	5
$SCS2_f$/Al STRIPS	$(0)_8$	2	2	2	2	6
NICALON SiC/6061 WIRES	0	18	5	18	5	5

The discontinuous SiC/Al was supplied by AFWL/Flight Dynamics Laboratory. All other metal matrix composites were supplied by The Aerospace Corporation.

Table 2. Gr/Al and Gr/Mg composites for on-orbit and laboratory thermal expansion measurements.

AEROSPACE MATERIAL NO.	MATERIAL DESCRIPTION FIBER/MATRIX/SURFACE FOIL	FLIGHT DATA	POST-FLIGHT LABORATORY DATA
AL3 - AL6	GY70/201/2024 (1 PLY, 0°)	LE & TE	LE, TE, & LC
AL7	GY70/201/2024 $(0,\pm60°)_S$	LE & TE	
AL12 & AL14	P55/6061/6061 (1 PLY, 0°)	LE & TE	LE, TE, & LC
AL15	P55/6061/6061 (1 PLY, 90°)	LE & TE	
AL33	P100/201/2024 $(\pm20°)_S$		LE & LC
MG3-MG6	P100/EZ33A/AZ31B (1 PLY, 0°)	LE & TE	LE, TE, & LC
MG9	P100/AZ91C/AZ61A (1 PLY, 0°)		LE & LC
MG10	P100/AZ91C/AZ61A $(\pm10°)_S$		LE & LC

LC = LABORATORY CONTROL, LE = LEADING EDGE, TE = TRAILING EDGE

Table 3. Postflight CTE data for Gr/Al composites.

MATERIAL DESCRIPTION	COEFFICIENT OF THERMAL EXPANSION, 10^{-6}/°F		
FIBER/MATRIX/SURFACE FOIL	LABORATORY CONTROL	LEADING EDGE	TRAILING EDGE
GY70/201/2024 (1 PLY, 0°)	3.5	3.2	3.8
P55/6061/6061 (1 PLY, 0°)	3.0	3.3	3.5
P100/201/2024 $(\pm 20°)_S$	1.2	1.1	

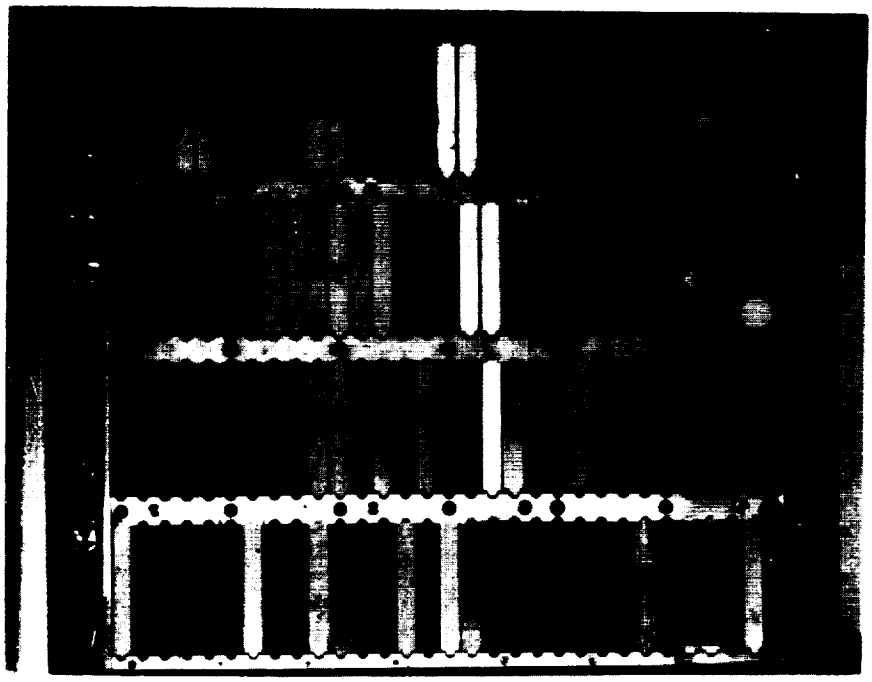

Figure 1. Postflight photograph of exposed side of leading edge cassette.

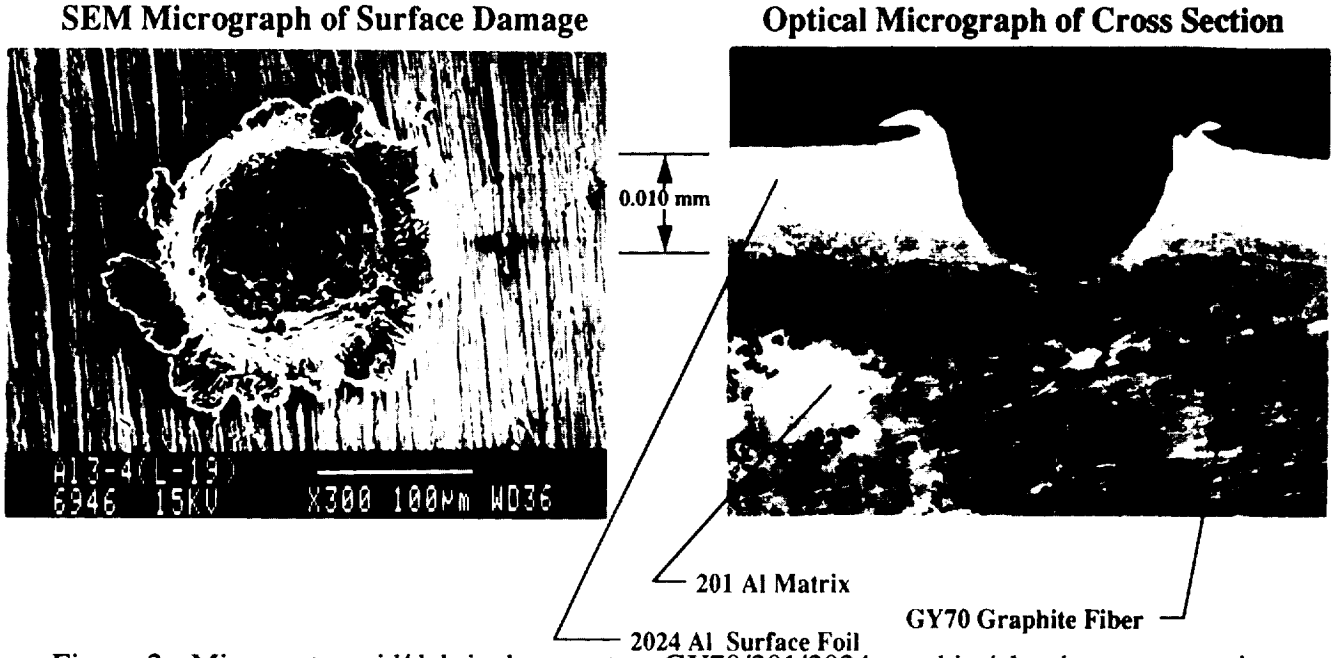

Figure 2. Micrometeoroid/debris damage to a GY70/201/2024 graphite/aluminum composite.

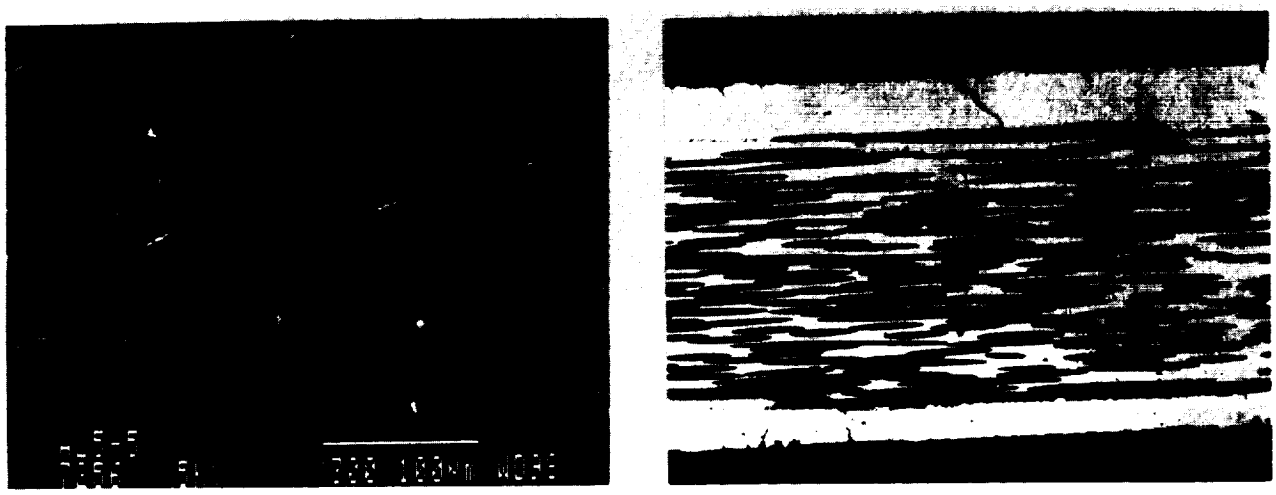

SEM Micrograph of Cracks in Surface Foil **Optical Micrograph of Cross Section**

Figure 3. Surface foil cracking of a GY70/201/2024 graphite/aluminum composite resulting from thermal fatigue of a brittle contaminated surface.

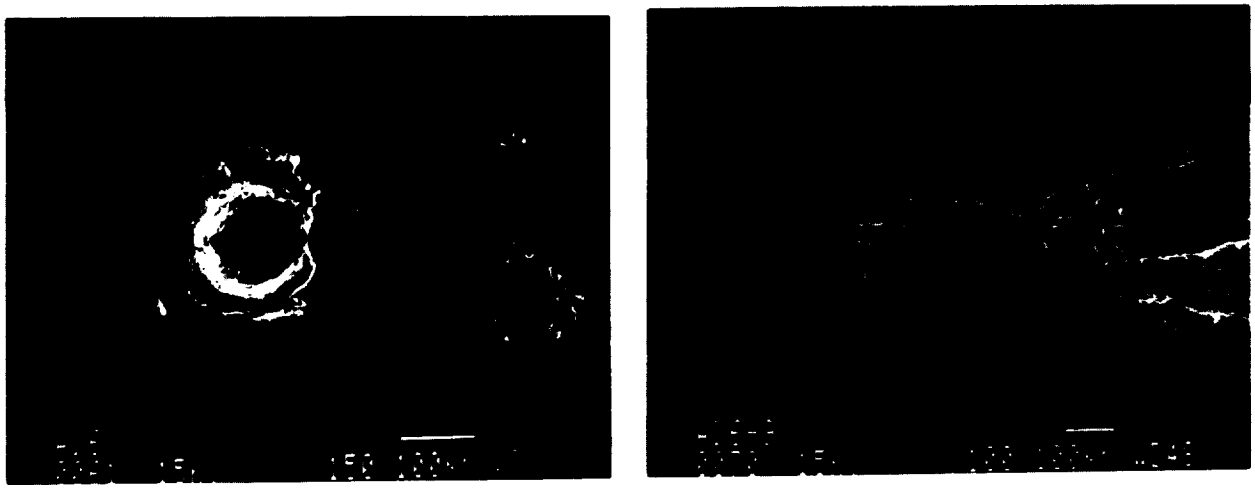

Figure 4. Isolated fatigue cracks that initiated at micrometeoroid craters and sample number engravings on the surface of GY70/201/2024 graphite/aluminum composites.

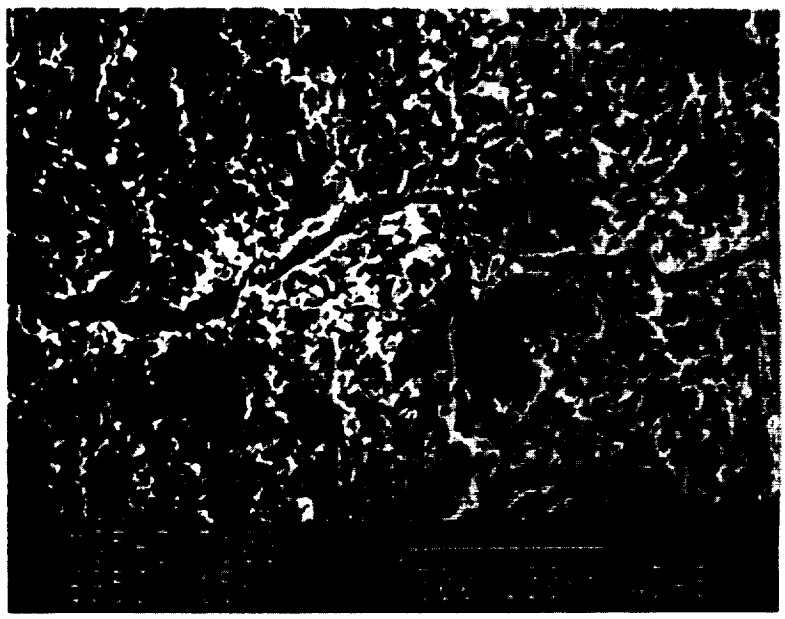

Figure 5. Scanning electron micrograph of a P100/EZ33A/AZ31B graphite/magnesium composite showing a fatigue crack that formed within a brittle oxide layer.

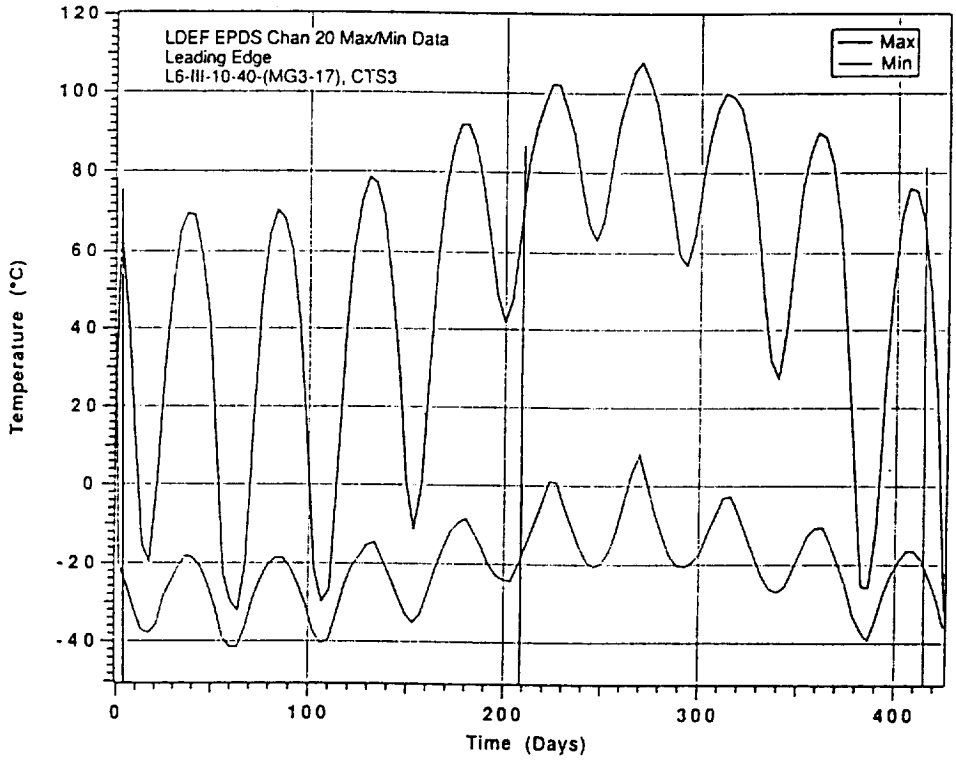

Figure 6. Maximum and minimum temperature recorded for each orbit for a P100/EZ33A/AZ31B Gr/Mg composite mounted on the leading edge of LDEF. Vertical lines indicate orbits selected for strain data analyses.

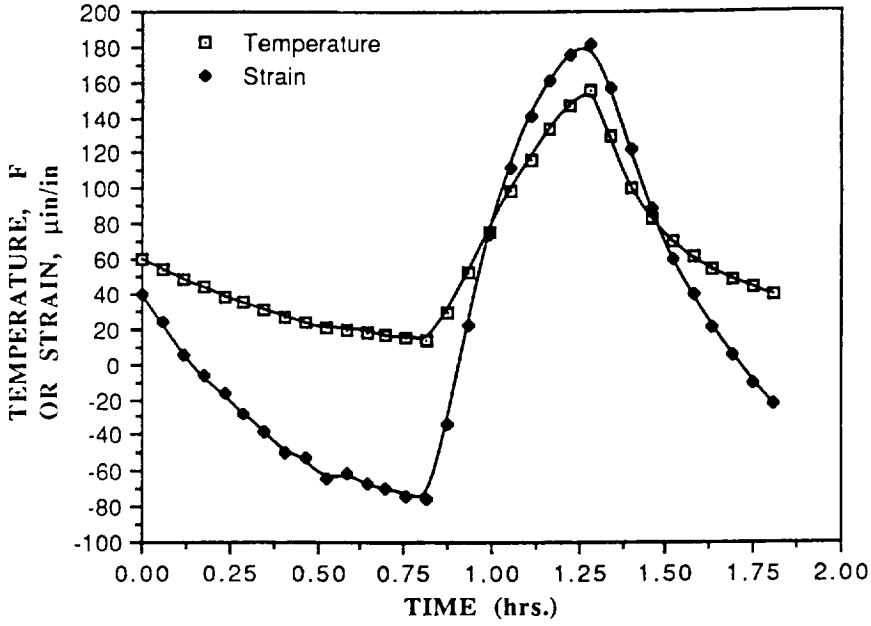

Figure 7. Flight data showing changes in temperature and strain as functions of time during one orbit for a P55/6061/6061 Gr/Al composite on the trailing edge.

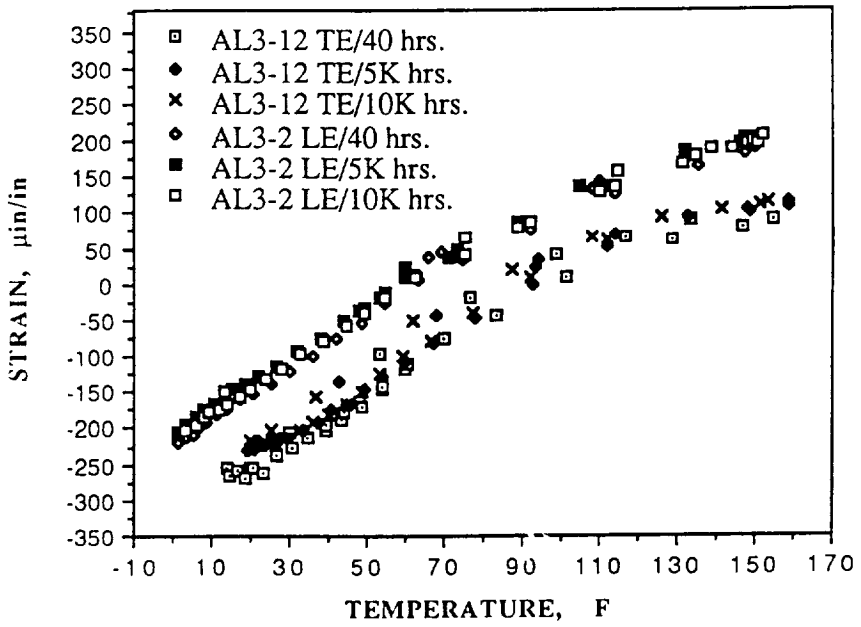

Figure 8. Flight data showing the change in strain as a function of temperature for GY70/201/ 2024 Gr/Al composites for three different orbits on the leading and trailing edges.

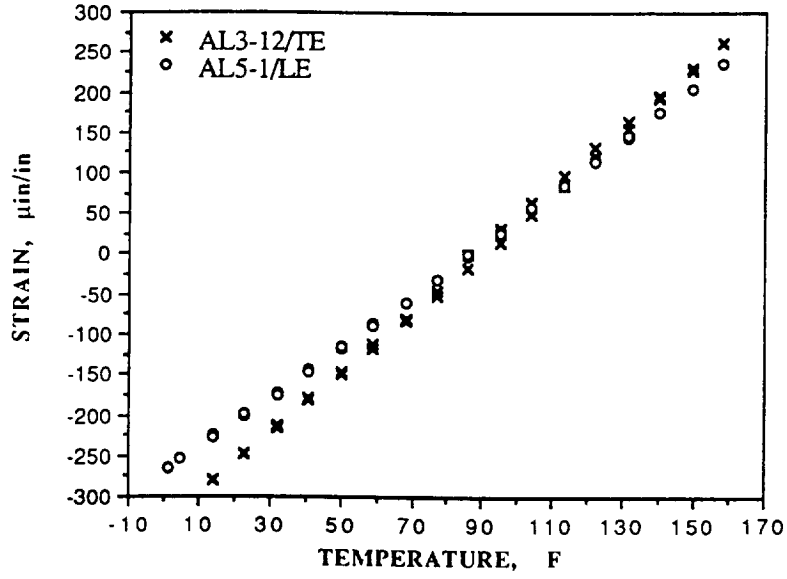

Figure 9. Postflight laser interferometer thermal expansion curves for leading and trailing edge GY70/201/2024 Gr/Al composites.

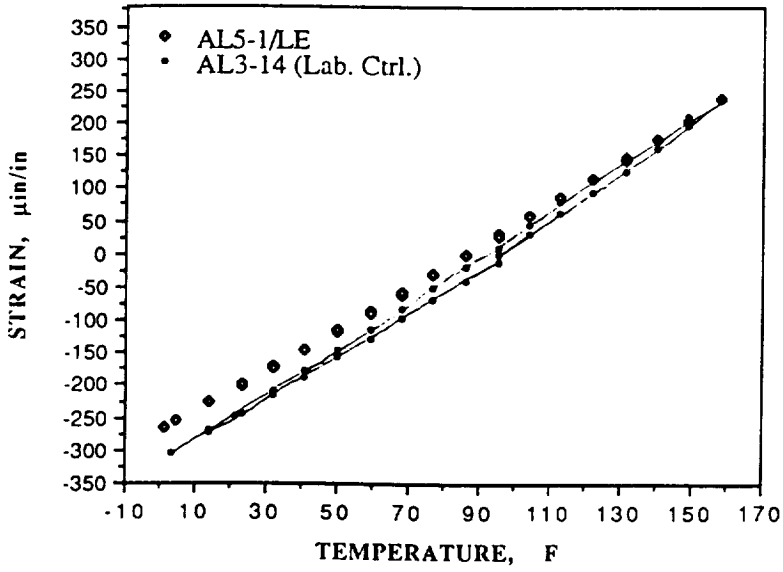

Figure 10. Postflight laser interferometer thermal expansion curves for leading edge and laboratory control GY70/201/2024 Gr/Al composites.

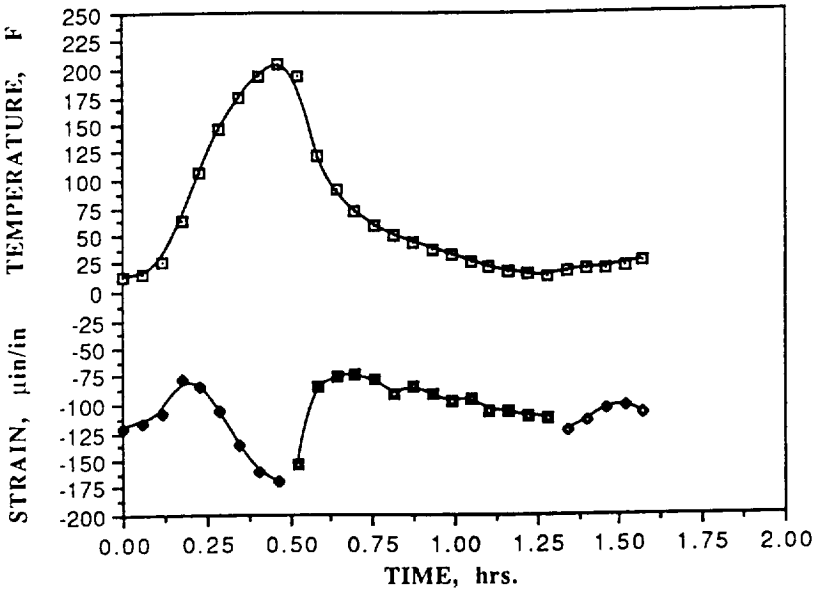

Figure 11. Flight data showing changes in temperature and strain as functions of time during one orbit for a P100/EZ33A/AZ31B Gr/Mg composite on trailing edge.

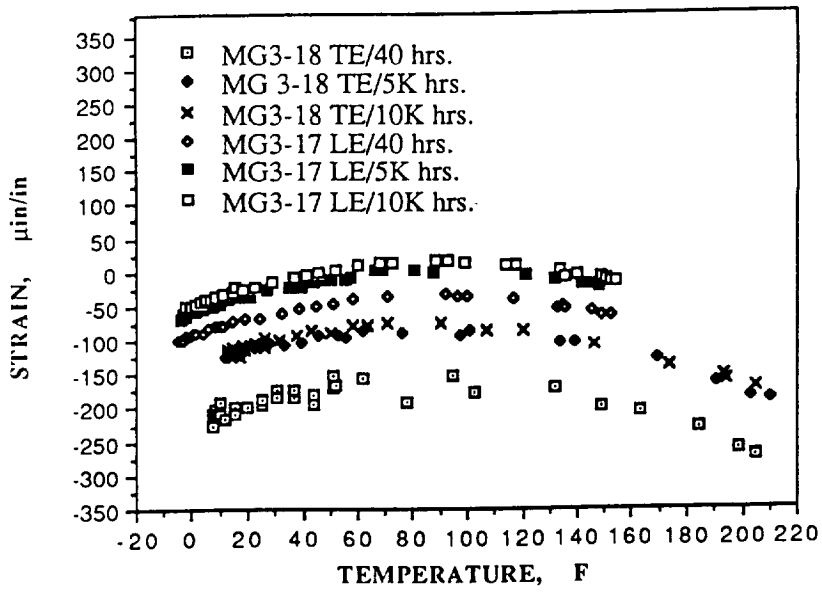

Figure 12. Flight data showing the change in strain as a function of temperature for P100/EZ33A/AZ31B Gr/Mg composites for three different orbits on the leading and trailing edges.

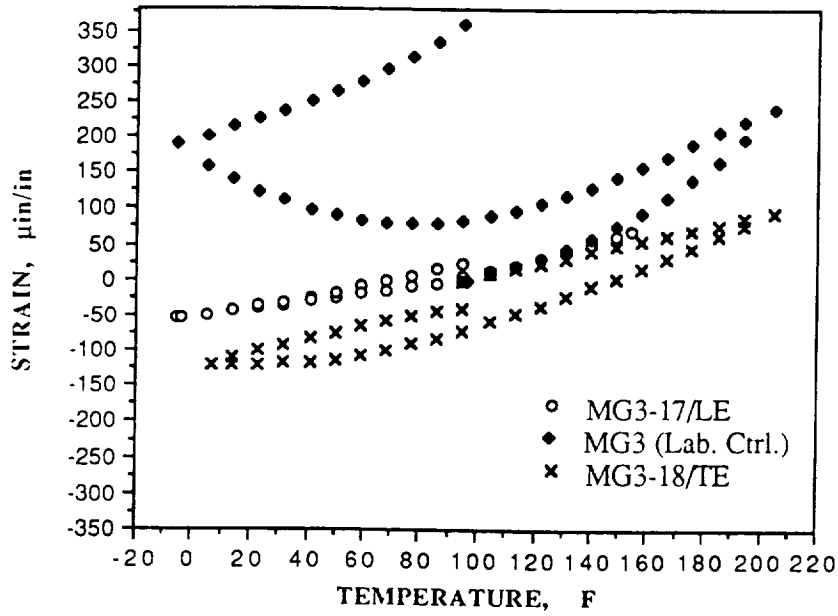

Figure 13. Postplight laser interferometer thermal expansion curves for leading and trailing edge and laboratory control P100/EZ33A/AZ31B Gr/Mg composites.

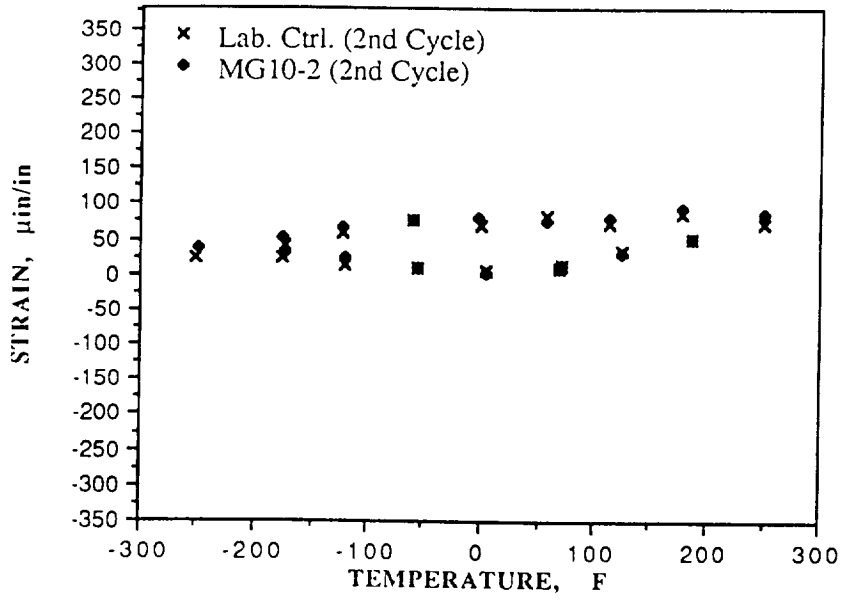

Figure 14. Postflight laser interferometer thermal expansion curves for leading edge and laboratory control P100/AZ91C/AZ61A $(\pm 10°)_S$ Gr/Mg composites.